INTERNATIONAL JOURNAL FOR NUMERICAL METHODS IN ENGINEERING
Int. J. Numer. Meth. Engng 2005; **62**:1606–1635
Published online 17 December 2004 in Wiley InterScience (www.interscience.wiley.com). DOI: 10.1002/nme.1236

Boundary element modelling of flat plate floors under vertical loading

Youssef F. Rashed*, †

Department of Structural Engineering, Cairo University, Giza, Egypt

SUMMARY

The present paper develops a boundary element model for flat plate floors. The floor slab is modelled using the shear-deformable plate bending theory. Internal columns or walls are treated using internal collocation technique, where three interaction generalized forces are considered at the slab–column connection: two bending moments in two directions and shear force in the vertical direction. Such forces are considered to be constant over the column cross-sections. The present technique takes into account the realistic geometric modelling of the column cross-sections. The effect of considering such geometry in the analysis of the bending moments transferred from slab to columns is studied. Several examples, including solution of practical building slab, are presented. The results are compared to those obtained from other numerical methods to demonstrate the accuracy and the reliability of the present formulation. The present formulation can be considered as an accurate tool to predict moment transferred from the slab to the column. Copyright © 2004 John Wiley & Sons, Ltd.

KEY WORDS: flat plate; boundary element method; slab–column connection; moment transfer; real geometry of columns

1. INTRODUCTION

Flat plate floors are commonly used in buildings due to several architectural requirements and other economical factors. The analysis of such structures is commonly carried out using the finite element method (FEM) [1] via several commercial packages. This is usually started by discretizing the slab domain into an appropriate mesh of plate-bending finite elements (usually the thin plate-bending element is used [1]). In case of modelling complicated geometries, engineers usually use CAD programs as pre-processing software to generate finite element meshes. Columns are modelled either to be rigid or as skeletal frame elements and linked to the slab at nodes [2]. Long walls or cores are usually modelled using the shell finite elements.

*Correspondence to: Y. F. Rashed, Department of Structural Engineering, Cairo University, Giza, Egypt.
†E-mail: youssef@eng.cu.edu.eg

Received 15 March 2004
Revised 27 July 2004
Accepted 7 September 2004

Such modelling enables the engineer to obtain several straining actions required to design the slab. However, it suffers from several disadvantages:

1. The need for using additional CAD software to model complex geometries, in many cases such meshing is carried out manually when dealing with long walls, leads to tremendous effort.
2. The obtained deflections (which are used to check for the building serviceability) in case of using the thin plate theory could be different from the actual one due to the shear-deformations [3]. Several FEM packages had overcome this disadvantage by implementing a suitable thick plate-bending element in their code.
3. The post-processing procedures are sometimes difficult, because the obtained results are given at nodes and usually the values of bending moments are given as the average value of the elements connected at the considered common node. When the common node is connected to the column, such an average value does not present a correct result as it ignores the drop of the bending moment transferred from the slab to the column.
4. The column real geometry and orientation are taken into consideration via the section properties of the column (area, moment of inertia, etc.). However, the real geometric representations of such columns in the FEM mesh are ignored. Such factors could greatly affect the results [4]. Several techniques were developed to take these factors into consideration such as using finer discretization over columns or by distributing the column stiffness over several nodes (see for example References [5, 6]); however, most of these techniques are difficult to be used practically among engineers in design companies.
5. The checking of the design or re-design after construction due to some changes in the column position or orientation, slab geometry, opening placements, etc. usually requires re-meshing and new analysis.
6. The testing of several alternatives for columns, walls, core positions and shapes to obtain minimum cost is difficult for complex geometries as it requires re-meshing several times.
7. The treatment of complex loading geometry such as computation of nodal forces results from applied loading of curved wall over the slab domain becoming very tedious.
8. The main outputs of such models are the straining actions and generalized displacements of the field slab. However, in most cases, the transferred moment from slab to column is ignored or roughly computed.

When columns became elongated in one direction in the building plane, the load transfer pattern changes [4]. In other words, the slab behaves as one-way slab (no longer a two-way slab [4]). Moreover a certain pattern of column or wall real geometry of cross-sections could be considered to totally change the values of bending moments transferred from slab to column. Recently, researchers have realized such facts as given in References [7, 8].

The boundary element method [9] (BEM) is an alternative technique (sometimes less general) to the FEM. Such a technique is employed by researchers in several engineering applications. Most of the research in the BEM is of a theoretical nature. It has been recognized recently that such a technique could overcome several drawbacks of the FEM especially in problems such as crack growth, cathode protection and infinite soil problems. Several commercial packages have developed to offer an end-user solution for such problems. However, to the author's knowledge (see a recent review paper by the author [10]) in the area of the analysis of building floors, such practical or end-user solution software has never been developed yet.

The application of the BEM to plate-bending problems modelled using the thin plate theory was introduced by Bézine [11] and Stern [12]. Vander Weeën [13] derived a BEM for the plate-bending problem based on the shear deformable plate theory according to Reissner [3].

Bézine [14] extended his formulation in Reference [11] to treat plates with internal conditions. The formulation in Reference [14] considers the internal conditions to resist using axial stiffness only. Such a formulation was improved by several researchers in the literature to model building slabs, as follows.

Hartmann [15] developed a BEM formulation for analysis of building slabs and the internal columns were treated as point concentrated loads. Such formulation cannot compute values over columns, due to the singularity nature of the BEM solution, which makes the formulation impractical.

de Paiva and Venturini [16–18] developed an alternative formulation to model columns by treating their effect as linear loading. Such formulation is more practical than that of Hartmann [15] as it could be used to compute values over columns. The formulation in References [16–18] takes into account the column bending stiffness. However, it computes only the axial force of the columns. In Reference [19], Oliveira Netoa and de Paiva improved the thin plate formulation presented in References [16–18] using three degrees of freedom per node. Still the formulation of Reference [19] does not compute column bending moments. Examples presented in References [16–19] are small and contain buildings of maximum four columns (which is not practical).

Hartley and Abdel-Akher [20, 21] used an alternative column model, which is similar to the point model of Hartmann [15] but they represented the column by five internal points. They modelled the column interaction forces to the slab by several combinations of these concentrated loading sets to simulate shear force and bending moments in the two directions. Still the formulation of References [20, 21] cannot predict values over columns due to the singularity that appears when using concentrated loads.

It has to be noted that the above formulations are not suitable for practical applications in structural engineering due to the following:

1. The use of the thin plate theory within the BEM (which employs a hyper-singular integral equation) not only ignores the shear deformation but it poorly models curved boundaries due to the change of the normal values at the element conjunction. Moreover, it requires computing hyper-singular integrals.
2. The use of concentrated loads in the modelling prohibits the computation of the values over columns.
3. The models presented above are with regards to the behaviour of the field slab, whereas moments transferred from slab to column are ignored. It has to be noted that such values of bending moments are of great influence in the structural design of the overall building.

On the other hand, in the area of research developments of the BEM using the shear-deformable plate-bending theory, only Rashed [22] proposed a BEM formulation to analyse plates with internal supports using the well-known flexibility approach. The formulation presented in Reference [22] considers only the axial stiffness of the columns. Extending such a formulation to treat bending stiffness is straightforward; however, it has not been reported yet. Despite the simplicity and versatility of the formulation presented in Reference [22], it

cannot treat plates having only free-edge boundary conditions, which occur in most cases in engineering practice.

The present paper develops a technique for modelling flat plate floors using the boundary element method together with the shear-deformable plate-bending theory, in which only the plate boundary (and openings, if any) is required to be discretized. Columns, internal walls or cores are modelled using internal cells to describe the real geometry of the cross-section. Three internal generalized forces are considered at each internal support: two bending moments in two directions and one shear force in the vertical direction. These generalized forces are considered to vary constantly over the column cross-section. In order to solve the problem, an additional three integral equations are written at each column centre. Such a formulation can model slabs with any boundary condition.

Several examples are presented including theoretical comparison against results of the BEM for the thin plate theory and results of analysis using the FEM. The effect of modelling the real geometry of column cross-section on the slab-column moment transfer scheme is also discussed. A practical example of building slab is demonstrated and results are compared with those obtained from FEM results. The analysed examples and the verification of the results confirm the reliability of using such a formulation in structural engineering practice.

2. BASIC BOUNDARY INTEGRAL EQUATIONS OF PLATES

Consider an arbitrary plate of domain Ω and boundary Γ, loaded by domain loading of intensity q. The plate is lying in the $x_1 - x_2$ plane where $x_3 = 0$ is located at the mid surface of the plate as shown in Figure 1. The indecial notation is used in this paper where the Greek indexes vary from 1 to 2 and Roman indexes vary from 1 to 3. The Reissner plate bending theory [3] is used in the present formulation. The direct boundary integral equation for such a plate can

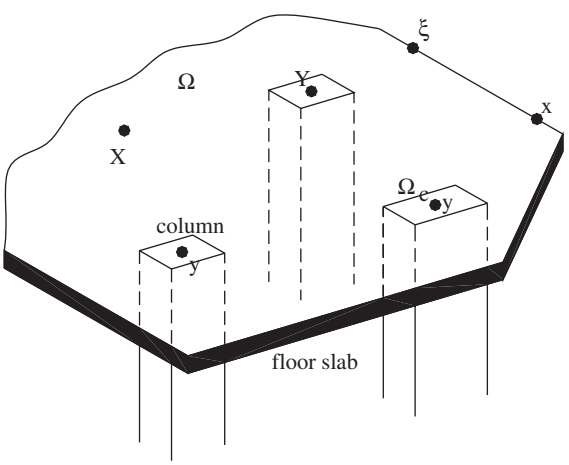

Figure 1. Geometry of the considered plate.

be written in the following form [13]:

$$C_{ij}(\xi)u_j(\xi) + \int_{\Gamma(\boldsymbol{x})} T_{ij}(\xi, \boldsymbol{x})u_j(\boldsymbol{x})\,\mathrm{d}\Gamma(\boldsymbol{x}) = \int_{\Gamma(\boldsymbol{x})} U_{ij}(\xi, \boldsymbol{x})t_j(\boldsymbol{x})\,\mathrm{d}\Gamma(\boldsymbol{x}) + \int_{\Gamma(\boldsymbol{x})} \left[V_{i,n}(\xi, \boldsymbol{x}) - \frac{v}{(1-v)\lambda^2} U_{i\alpha}(\xi, \boldsymbol{x}) \right] q\,\mathrm{d}\Gamma(\boldsymbol{x}) \tag{1}$$

where $T_{ij}(\xi, \boldsymbol{x})$ and $U_{ij}(\xi, \boldsymbol{x})$ are the two-point fundamental solution kernels for tractions and displacements, respectively [13]. The two points ξ and $\boldsymbol{x}$ are the source and the field points, respectively. $u_j(\boldsymbol{x})$ and $t_j(\boldsymbol{x})$ denote the boundary generalized displacements and tractions. $C_{ij}(\xi)$ is the jump term and the kernel $V_i(\xi, \boldsymbol{x})$ is a suitable particular solution to represent domain loading [13]. The symbols v and λ denote the plate Poisson's ratio and shear factor. After discretizing the plate boundary to *NE* quadratic boundary elements, Equation (1) could be written in matrix form as follows [3]:

$$\begin{bmatrix} \mathbf{A} \\ 3\mathrm{N} \times 3\mathrm{N} \end{bmatrix} \begin{Bmatrix} \mathbf{b} \\ 3\mathrm{N} \times 1 \end{Bmatrix} = \begin{Bmatrix} \mathbf{RHS_b} \\ 3\mathrm{N} \times 1 \end{Bmatrix} \tag{2}$$

where matrix [**A**] denotes the matrix of coefficients, vector {**b**} denotes the vector of unknown boundary values and vector {$\mathbf{RHS_b}$} denotes the vector of the known boundary conditions on the right-hand side of the equation. Equation (2) could be solved to obtain the unknown boundary values.

Stress resultants (bending moments $M_{\alpha\beta}$ and shear forces $Q_{3\beta}$) can be computed at any internal field point ξ as follows [13]:

$$M_{\alpha\beta}(\xi) = \int_{\Gamma(\boldsymbol{x})} U_{\alpha\beta k}(\xi, \boldsymbol{x})t_k(\boldsymbol{x})\,\mathrm{d}\Gamma(\boldsymbol{x}) - \int_{\Gamma(\boldsymbol{x})} T_{\alpha\beta k}(\xi, \boldsymbol{x})u_k(\boldsymbol{x})\,\mathrm{d}\Gamma(\boldsymbol{x}) + q\int_{\Gamma(\boldsymbol{x})} W_{\alpha\beta}(\xi, \boldsymbol{x})\,\mathrm{d}\Gamma(\boldsymbol{x}) + \frac{v}{(1-v)\lambda^2} q\,\delta_{\alpha\beta} \tag{3}$$

$$Q_{3\beta}(\xi) = \int_{\Gamma(\boldsymbol{x})} U_{3\beta k}(\xi, \boldsymbol{x})t_k(\boldsymbol{x})\,\mathrm{d}\Gamma(\boldsymbol{x}) - \int_{\Gamma(\boldsymbol{x})} T_{3\beta k}(\xi, \boldsymbol{x})u_k(\boldsymbol{x})\,\mathrm{d}\Gamma(\boldsymbol{x}) + q\int_{\Gamma(\boldsymbol{x})} W_{3\beta}(\xi, \boldsymbol{x})\,\mathrm{d}\Gamma(\boldsymbol{x}) \tag{4}$$

where the new kernels U_{ijk}, T_{ijk} and $W_{i\beta}$ are the derivatives of the kernels in Equation (1) and can be obtained from Reference [13]. Figure 2 shows the positive directions of such stress resultants.

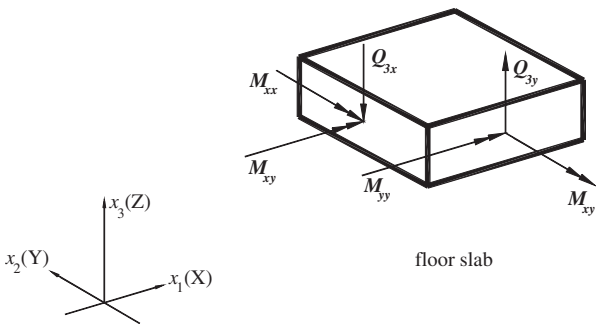

Figure 2. Positive directions for the stress resultants in the floor slab.

3. THE PROPOSED FLAT PLATE MODELLING

In this paper, it is assumed that columns (or walls or cores) are connected to the slab over distributed patches (see Figure 1) to represent the real geometry of the column cross-section. Three interaction forces are considered: two bending moments in the two directions and one vertical shear. In order to model the rigidity of the columns or walls, the interaction forces are assumed to vary constantly over the column cross-section. If a series of column generalized forces are applied over the plate domain, Equation (1) could be re-written in the following form:

$$C_{ij}(\xi)u_j(\xi) + \int_{\Gamma(\boldsymbol{x})} T_{ij}(\xi, \boldsymbol{x})u_j(\boldsymbol{x})\,\mathrm{d}\Gamma(\boldsymbol{x}) = \int_{\Gamma(\boldsymbol{x})} U_{ij}(\xi, \boldsymbol{x})t_j(\boldsymbol{x})\,\mathrm{d}\Gamma(\boldsymbol{x})$$
$$+ \int_{\Gamma(\boldsymbol{x})} \left[V_{i,n}(\xi, \boldsymbol{x}) - \frac{v}{(1-v)\lambda^2} U_{i\alpha}(\xi, \boldsymbol{x}) \right] q\,\mathrm{d}\Gamma(\boldsymbol{x})$$
$$+ \sum_c \left\{ \int_{\Omega_c(\boldsymbol{y})} \left[U_{ik}(\xi, \boldsymbol{y}) - \frac{v}{(1-v)\lambda^2} U_{i\alpha,\alpha}(\xi, \boldsymbol{y})\delta_{3k} \right] F_k(y)\,\mathrm{d}\Omega_c(\boldsymbol{y}) \right\} \tag{5}$$

where c denotes the number of internal columns that have domain Ω_c, F_k denotes the columns two bending moments ($F_1 = M_{xx}$, $F_2 = M_{yy}$) and column vertical force ($F_3 = F$). Field point y denotes the point of the internal column centre. Figure 2 shows the positive directions for the column generalized forces. The column forces $F_k(y)$ can be expressed in terms of the column stiffness coefficients as follows:

$$F_k(y) = \frac{-u_k(y)S_k(y)}{A(y)} \quad \text{(no summation on } k\text{)} \tag{6}$$

where S_k represents the bending and the axial stiffness of the column which are given, for prismatic column by

$$S_1(y) = B(y)\left[\frac{4EI_{x_2}}{L}\right]_{\text{top}} + \left[\frac{4EI_{x_2}}{L}\right]_{\text{bottom}} \tag{7}$$

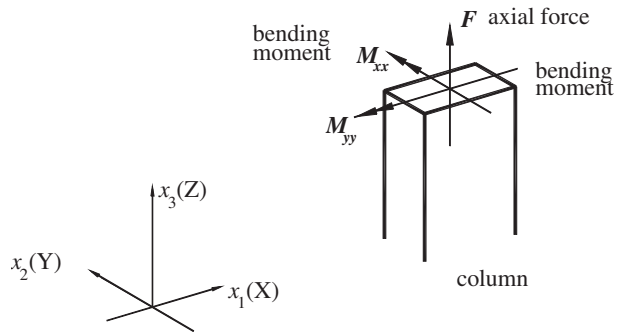

Figure 3. Positive directions for column generalized forces.

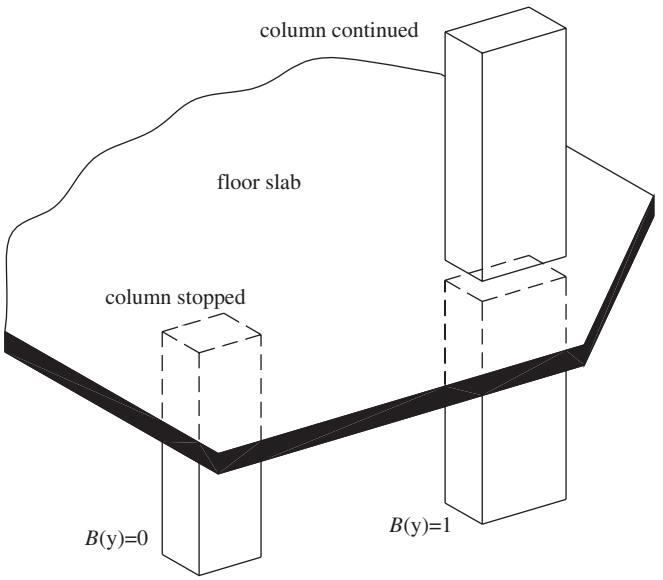

Figure 4. Value of the coefficient $B(\boldsymbol{y})$ for different columns.

$$S_2(y) = B(y)\left[\frac{4EI_{x_1}}{L}\right]_{\text{top}} + \left[\frac{4EI_{x_1}}{L}\right]_{\text{bottom}} \tag{8}$$

and

$$S_3(y) = B(y)\left[\frac{EA}{L}\right]_{\text{top}} + \left[\frac{EA}{L}\right]_{\text{bottom}} \tag{9}$$

where E, Ix_α, A and L denote modulus of elasticity, moment of inertial about the axis x_α, area and length of the column, respectively. The coefficient $B(y)$ can take either zero to represent that the column ends at the considered floor or one if the column be continues to the top floor (see Figure 4). It has to be noted that Equations (7)–(9) are adjusted to match the definitions and positive directions between plate and column as shown in Figures 2 and 3.

In case of having the column with different cross-sections at the bottom and top floors, the modelling of such column can be easily carried out by representing it using two different columns and all equations presented herein are still valid. Equations (7)–(9) could be adjusted to match any stiffness when having a column with non-prismatic cross-section or columns with different end conditions. It has to be noted that, in case of having a long column, wall, or core, the cross-section of such a support can be modelled using more than one internal cell.

Substituting from Equation (6) into the integral equation in (5), the last term can be easily written as follows (noting that the values of the column generalized forces are assumed to vary constantly over each column cross-section):

$$\int_{\Omega_c(\boldsymbol{y})} \left[U_{ik}(\xi, \boldsymbol{y}) - \frac{v}{(1-v)\lambda^2} U_{i\alpha,\alpha}(\xi, \boldsymbol{y})\delta_{3k} \right] F_k(y)\, \mathrm{d}\Omega_c(\boldsymbol{y})$$

$$= \left\{ \int_{\Omega_c(\boldsymbol{y})} \left[U_{ik}(\xi, \boldsymbol{y}) - \frac{v}{(1-v)\lambda^2} U_{i\alpha,\alpha}(\xi, \boldsymbol{y})\delta_{3k} \right] \mathrm{d}\Omega_c(\boldsymbol{y}) \right\} F_k(y) \tag{10}$$

$$= \left\{ \int_{\Omega_c(\boldsymbol{y})} \left[U_{ik}(\xi, \boldsymbol{y}) - \frac{v}{(1-v)\lambda^2} U_{i\alpha,\alpha}(\xi, \boldsymbol{y})\delta_{3k} \right] \mathrm{d}\Omega_c(\boldsymbol{y}) \right\}$$

$$\times \left[\frac{-u_k(\boldsymbol{y}) S_k(\boldsymbol{y})}{A(\boldsymbol{y})} - q\,\delta_{3k} B(\boldsymbol{y}) \right] \tag{11}$$

It can be seen that the last term ($q\,\delta_{3k} B(y)$) of the former Equation (11) is introduced to the equation, which represents the value of the domain load part over the column cross-section. Such a value should be subtracted when the column continues to the top floor (i.e. $B(y) = 1$).

After replacing the last term in Equation (5) by the result of Equation (11), Equation (5) contains three unknowns at each boundary node and an additional three unknowns at each internal column centre. If such an equation is written for each degree of freedom at each boundary node, the number of unknowns will be more than the number of equations. In order to generate another equation, a collocation scheme is carried out at each internal column centre to give (recall Equations (5) and (11) and replace ξ by $\boldsymbol{Y}$):

$$u_i(\boldsymbol{Y}) + \int_{\Gamma(\boldsymbol{x})} T_{ij}(\boldsymbol{Y}, \boldsymbol{x}) u_j(\boldsymbol{x})\, \mathrm{d}\Gamma(\boldsymbol{x}) = \int_{\Gamma(\boldsymbol{x})} U_{ij}(\boldsymbol{Y}, \boldsymbol{x}) t_j(\boldsymbol{x})\, \mathrm{d}\Gamma(\boldsymbol{x})$$

$$+ \int_{\Gamma(\boldsymbol{x})} \left[V_{i,n}(\boldsymbol{Y}, \boldsymbol{x}) - \frac{v}{(1-v)\lambda^2} U_{i\alpha}(\boldsymbol{Y}, \boldsymbol{x}) \right] q\, \mathrm{d}\Gamma(\boldsymbol{x})$$

$$+ \sum_c \left\{ \int_{\Omega_c(\boldsymbol{y})} \left[U_{ik}(\boldsymbol{Y}, \boldsymbol{y}) - \frac{v}{(1-v)\lambda^2} U_{i\alpha,\alpha}(\boldsymbol{Y}, \boldsymbol{y})\delta_{3k} \right] \mathrm{d}\Omega_c(\boldsymbol{y}) \right\}$$

$$\times \left[\frac{-u_k(y) S_k(y)}{A(y)} - q\,\delta_{3k} B(y) \right] \tag{12}$$

where $\boldsymbol{Y}$ is a new source point located at each column centre. Equation (5) together with Equations (11) and (12) can be used to solve the problem.

4. GENERALIZED DISPLACEMENTS AND STRAINING ACTIONS AT INTERNAL POINTS

After the solution of Equations (5), (11) and (12), all boundary values (generalized displacements and tractions) will be known. Values of generalized displacements at column centres will also be known. Column forces can be computed easily using Equation (6). Generalized displacements at internal points could be obtained using Equation (12) by replacing $\boldsymbol{Y}$ by ξ to denote the arbitrary internal point. Straining actions, on the other hand, at internal point ξ could be obtained by modifying the integral Equations in (3) and (4) to include the effect of the generalized column force terms to give

$$\begin{aligned} M_{\alpha\beta}(\xi) = & \int_{\Gamma(\boldsymbol{x})} U_{\alpha\beta k}(\xi, \boldsymbol{x}) t_k(\boldsymbol{x})\, \mathrm{d}\Gamma(\boldsymbol{x}) - \int_{\Gamma(\boldsymbol{x})} T_{\alpha\beta k}(\xi, \boldsymbol{x}) u_k(\boldsymbol{x})\, \mathrm{d}\Gamma(\boldsymbol{x}) \\ & + q \int_{\Gamma(\boldsymbol{x})} W_{\alpha\beta}(\xi, \boldsymbol{x})\, \mathrm{d}\Gamma(\boldsymbol{x}) + \frac{v}{(1-v)\lambda^2}\, q\delta_{\alpha\beta} \\ & + \sum_c \left\{ \int_{\Omega_c(\boldsymbol{y})} \left[U_{\alpha\beta k}(\xi, \boldsymbol{y}) - \frac{v}{(1-v)\lambda^2}\, U_{\alpha\beta\theta,\theta}(\xi, \boldsymbol{y}) \delta_{3k} \right] \mathrm{d}\Omega_c(\boldsymbol{y}) \right\} \\ & \times \left[\frac{-u_k(y) S_k(y)}{A(y)} - q\delta_{3k} B(y) \right] \end{aligned} \tag{13}$$

and

$$\begin{aligned} Q_{3\beta}(\xi) = & \int_{\Gamma(\boldsymbol{x})} U_{3\beta k}(\xi, \boldsymbol{x}) t_k(\boldsymbol{x})\, \mathrm{d}\Gamma(\boldsymbol{x}) - \int_{\Gamma(\boldsymbol{x})} T_{3\beta k}(\xi, \boldsymbol{x}) u_k(\boldsymbol{x})\, \mathrm{d}\Gamma(\boldsymbol{x}) \\ & + q \int_{\Gamma(\boldsymbol{x})} W_{3\beta}(\xi, \boldsymbol{x})\, \mathrm{d}\Gamma(\boldsymbol{x}) \\ & + \sum_c \left\{ \int_{\Omega_c(\boldsymbol{y})} \left[U_{3\beta k}(\xi, \boldsymbol{y}) - \frac{v}{(1-v)\lambda^2}\, U_{3\beta\theta,\theta}(\xi, \boldsymbol{y}) \delta_{3k} \right] \mathrm{d}\Omega_c(\boldsymbol{y}) \right\} \\ & \times \left[\frac{-u_k(y) S_k(y)}{A(y)} - q\delta_{3k} B(y) \right] \end{aligned} \tag{14}$$

The relevant new kernel derivatives are given in Reference [22]. It has to be noted that all kernels at internal points are smooth, and could be straightforwardly computed even over column centres (the singular source point). The last integral of Equation (13) contains a kernel having strong singularity. Fortunately, the jump term that results from such integral has vanished, and the integral is computed in the sense of Cauchy principle value.

5. NUMERICAL IMPLEMENTATION

The boundary of the considered slab is divided into *NE* quadratic elements having *N* nodes. Each column or internal wall or core is represented by a constant internal cell. Equations (5), (11) and (12) can be re-written in matrix form as follows:

$$\begin{bmatrix} \mathbf{A} & \mathbf{A_2} \\ 3\mathrm{N} \times 3\mathrm{N} & 3N \times 3N_c \\ \mathbf{A_1} & \mathbf{A_3} \\ 3N_c \times 3N & 3N_c \times 3N_c \end{bmatrix} \begin{Bmatrix} \mathbf{b} \\ 3\mathrm{N} \times 1 \\ \mathbf{c} \\ 3N_c \times 1 \end{Bmatrix} = \begin{Bmatrix} \mathbf{RHS_b} \\ 3\mathrm{N} \times 1 \\ \mathbf{RHS_c} \\ 3N_c \times 1 \end{Bmatrix} \tag{15}$$

where matrix [**A**] and vector {**b**} are previously defined in Equation (2). The additional matrices are defined as follows:

From Equation (12), matrix [$\mathbf{A_1}$] contains the coefficients of the following integrals, when the collocation point is located at column centre $\boldsymbol{Y}$

$$[\mathbf{A_1}] = \sum_{NE} \int_{\text{element}} T_{ij}(\boldsymbol{Y}, \boldsymbol{x}) \Phi \, \mathrm{d}\Gamma(\boldsymbol{x}) \quad \text{or} \quad \sum_{NE} \int_{\text{element}} U_{ij}(\boldsymbol{Y}, \boldsymbol{x}) \Phi \, \mathrm{d}\Gamma(\boldsymbol{x}) \tag{16}$$

where Φ denote the element shape functions. The choice between the above two integrals is dependent on the applied boundary conditions using the same procedures as that when computing [**A**] matrix (see Reference [9] for details).

From Equation (11), matrix [$\mathbf{A_2}$] contains the coefficients of the following integrals, when the collocation point is located at a boundary source point ξ:

$$[\mathbf{A_2}] = \sum_{c} \left\{ \int_{\Omega_c(\boldsymbol{y})} \left[U_{ik}(\xi, \boldsymbol{y}) - \frac{v}{(1-v)\lambda^2} U_{i\alpha,\alpha}(\xi, \boldsymbol{y}) \delta_{3k} \right] \mathrm{d}\Omega_c(\boldsymbol{y}) \right\} \times \left[\frac{-S_k(y)}{A(y)} \right] \tag{17}$$

From Equation (12), matrix [$\mathbf{A}_3$] contains the coefficients of the following integrals, when the collocation point is located at column centre $\boldsymbol{Y}$:

$$[\boldsymbol{A_3}] = \sum_{c} \left\{ \int_{\Omega_c(\boldsymbol{y})} \left[U_{ik}(\boldsymbol{Y}, \boldsymbol{y}) - \frac{v}{(1-v)\lambda^2} U_{i\alpha,\alpha}(\boldsymbol{Y}, \boldsymbol{y}) \delta_{3k} \right] \mathrm{d}\Omega_c(\boldsymbol{y}) \right\} \times \left[\frac{-S_k(y)}{A(y)} \right] + 1 \tag{18}$$

It has to be noted that the one at the end of the above equation is added to represent the value of the generalized displacement at the internal point $\boldsymbol{Y}$ (the term $u_i(\boldsymbol{Y})$ in Equation (12)).

The vector of the {$\mathbf{RHS}_c$} contains the following integrals (recall Equation (12)):

$$\begin{aligned} \{\mathbf{RHS}_c\} = & -\sum_{NE} \int_{\text{element}} \left[V_{i,n}(\boldsymbol{Y}, \boldsymbol{x}) - \frac{v}{(1-v)\lambda^2} U_{i\alpha}(\boldsymbol{Y}, \boldsymbol{x}) \right] q \, \mathrm{d}\Gamma(\boldsymbol{x}) \\ & + \sum_{c} \left\{ \int_{\Omega_c(\boldsymbol{y})} \left[U_{ik}(\boldsymbol{Y}, \boldsymbol{y}) - \frac{v}{(1-v)\lambda^2} U_{i\alpha,\alpha}(\boldsymbol{Y}, \boldsymbol{y}) \delta_{3k} \right] \mathrm{d}\Omega_c(\boldsymbol{y}) \right\} [q \delta_{3k} B(y)] \end{aligned} \tag{19}$$

Also it has to be noted that vector $\{\mathbf{RHS_b}\}$ has the same definition as that in Equation (2) in addition to the following term (recall Equation (11)):

$$\sum_c \left\{ \int_{\Omega_c(\mathbf{y})} \left[U_{ik}(\xi, \mathbf{y}) - \frac{v}{(1-v)\lambda^2} U_{i\alpha,\alpha}(\xi, \mathbf{y})\delta_{3k} \right] \mathrm{d}\Omega_c(\mathbf{y}) \right\} [q\delta_{3k}B(y)] \tag{20}$$

Vector $\{\mathbf{c}\}$ contains the unknown generalized displacements at the column centre points. It can be seen that by the solution of Equation (15) the boundary values together with values of generalized displacements at column centres could be determined.

6. NUMERICAL APPLICATIONS

In this section, the present formulation is tested using several parametric studies. The results are compared to results obtained from other numerical models. The examples will focus on both the behaviour of the field slab and the supporting columns. Quadratic boundary elements were used in the present analysis. The placements of the nodes are left arbitrary to allow modelling of discontinuous boundary conditions. Four Gauss points are used for the numerical integrations of the boundary elements, and 4×4 are used for integration over cells. A special technique of using element sub-division is used to treat quasi-singular integrals. Logarithmic singularities are treated using the non-linear co-ordinate transformation by Telles [23]. Strong singularities, on the other hand, are indirectly treated using the well-known rigid body technique described in Reference [9].

6.1. Verification example: comparison to BEM using the thin plate theory

In this example the plate in Figure 5 is considered with $L_1 = 12.5$ and $L_2 = 10$. The column dimensions are chosen to be 1×1 to match the dimensions considered in Reference [20].

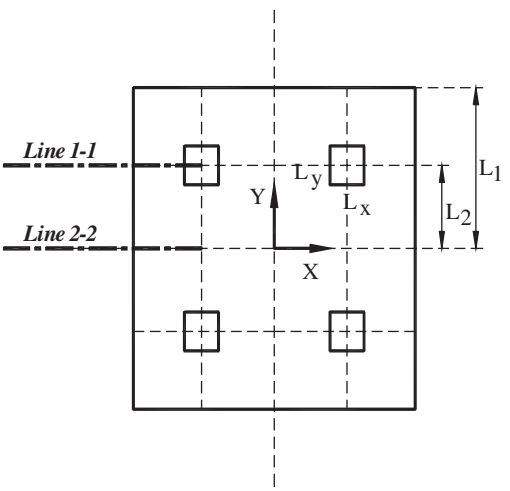

Figure 5. Geometry of the problem analysed in examples 1 and 2.

The following properties are used: $E = 480\,000$, $v = 0.35$ and the thickness of the slab was 0.5. The column length was 10 and stopped at the plate (i.e. $B(y) = 0$). It has to be noted that units in Reference [20] are not defined. Herein it is assumed that the given values have consistent units. The purposes of this example are

1. to demonstrate the results for a simple verification problem, and
2. to compare the results of the present formulation against those of the BEM using the thin plate theory of Reference [20].

In Reference [20], three models were considered:

- In model 1, the internal patches were assumed as totally rigid,
- In model 2, the patches were assumed as also rigid but by modelling them as holes inside the slab domain and placing 4 boundary elements to surround each hole with clamped boundary conditions and
- In model 3, both the plate and the supporting columns are modelled using the formulation presented in Reference [20], which employs the thin plate theory. Each side are modelled using six second-order boundary elements.

In the present analysis, two models are considered:

- The first model employs the present formulation considering the column actual stiffness (to be compared to model 3 in Reference [20]), and
- The second model is based on modelling the column as rigid patches (to be compared to model 1 and model 2 in Reference [20]). Four quadratic boundary elements were used on each side of the plate.

Figures 6–11 demonstrate the deflections and bending moments M_{xx} and M_{yy} at $y = 0$ and 9. It can be seen that the present formulation results are in good agreement with those of Reference [20]. The following notes could be concluded from these figures:

1. The results presented in Reference [20] were plotted at ($y = 0$) or near the column edges ($y = 9$), i.e. away from the column centres (column are located at $y = 9.5$ to $y = 10.5$). This is mainly due to the formulation presented in Reference [20] not being

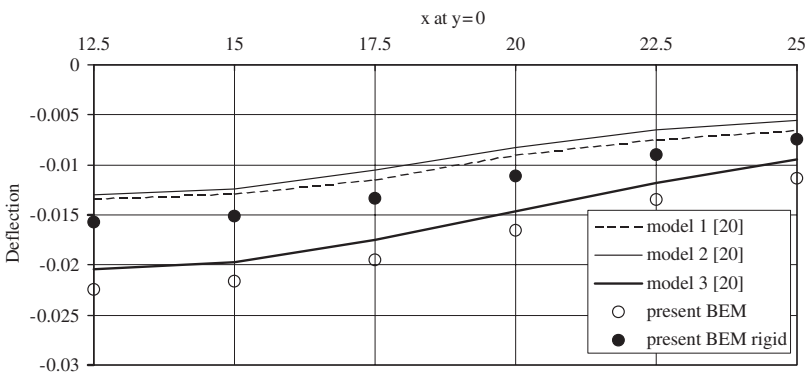

Figure 6. Deflection along x-axis at $y = 0$.

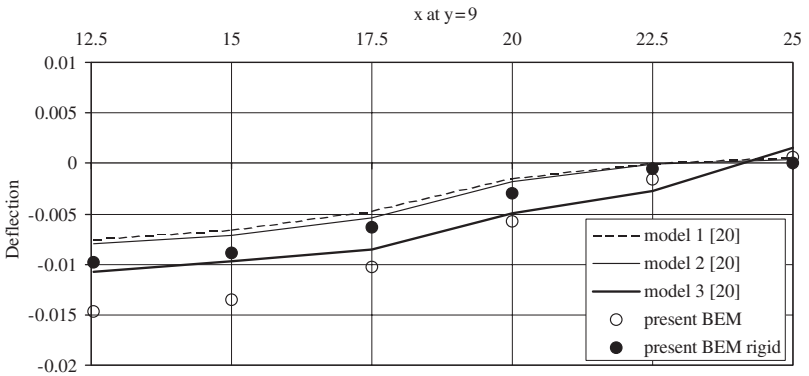

Figure 7. Deflection along x-axis at $y = 9$.

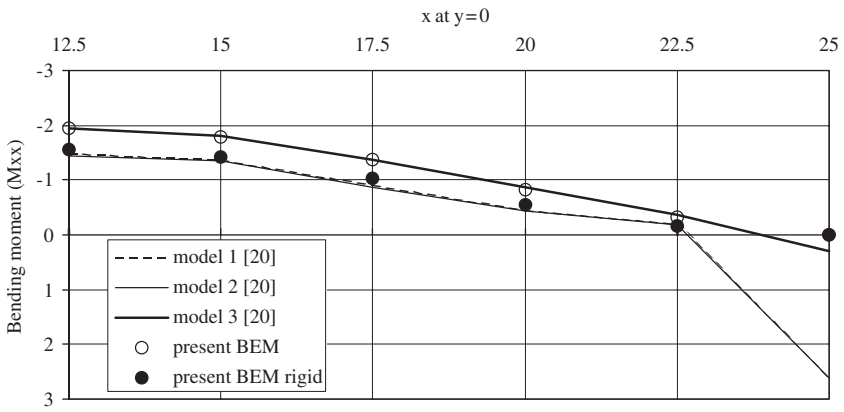

Figure 8. Bending moment M_{xx} along x-axis at $y = 0$.

capable computing values over columns due to the singularity of the model used in Reference [20].

2. In Reference [20] special second-order boundary elements were used to model the problem. This is mainly due to the used free-edge boundary conditions. Such a case could be easily solved using the traditional quadratic elements with high accuracy when employing the shear-deformable plate-bending theory as demonstrated in the present model.
3. Several values of the M_{xx} are not zero at the free edge in the results of Reference [20], whereas they are absolutely zero in the present formulation. On the other hand, values of M_{yy} are overshooting, which is not the case in the present formulation.
4. Always values of bending moments obtained from FEM (obtained from Reference [20]) and BEM (results of the present formulation) are closer than those for the deflections. This is due to the use of different plate-bending theories as mentioned before in the Introduction and in References [13, 22].

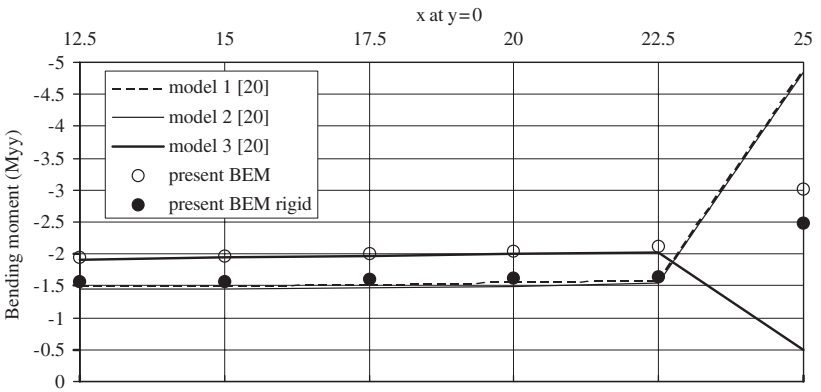

Figure 9. Bending moment M_{yy} along x-axis at $y = 0$.

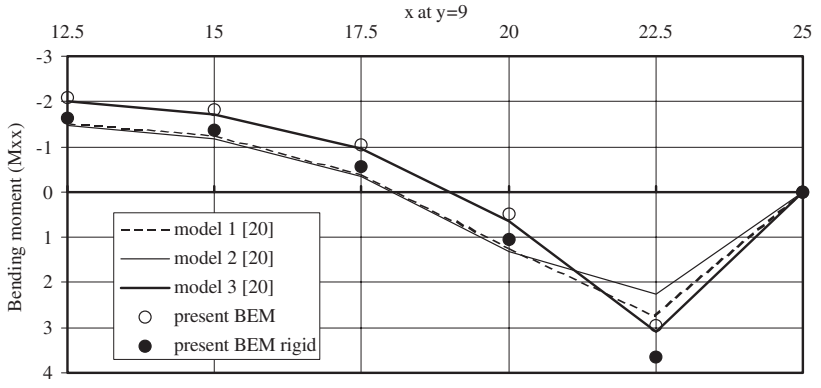

Figure 10. Bending moment M_{xx} along x-axis at $y = 9$.

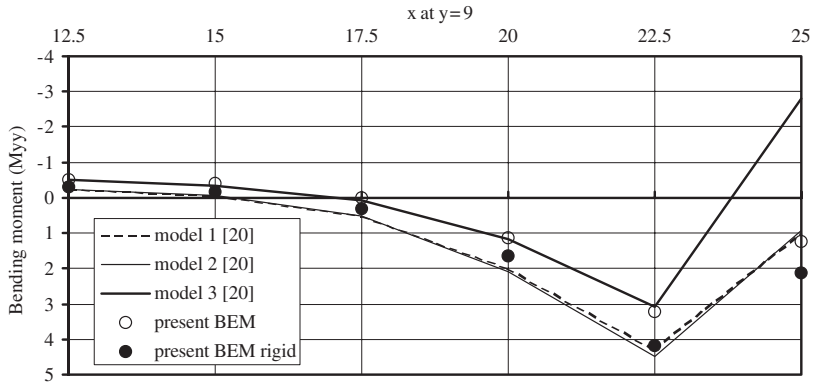

Figure 11. Bending moment M_{yy} along x-axis at $y = 9$.

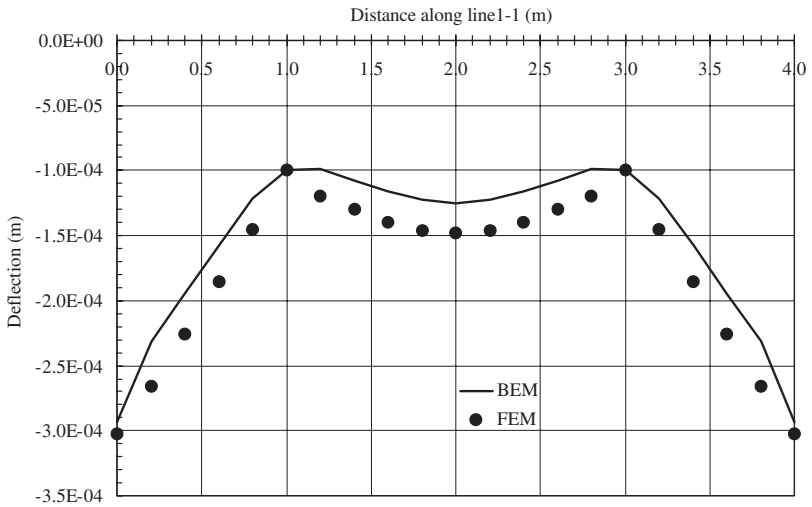

Figure 12. Deflection distribution along line 1-1 ($t = 0.4$).

6.2. Verification example: comparison to finite element modelling

The purpose of this example is to demonstrate a comparison between the results obtained from the present formulation against results of the finite element method. The example will focus on both the field deflections and bending moments in the slab as well as the moment transferred from the slab to the column, which is usually not considered by researchers in the literature.

The same slab shown in Figure 5 is reconsidered in this example with $L_1 = 4\,\text{m}$ and $L_2 = 3\,\text{m}$. The slab is discretized using 16×16 finite elements (four-noded rectangular elements are used) and 3×3 boundary elements (quadratic elements). Both the BEM and FEM use the shear-deformable plate-bending theory.

Figures 12–23 demonstrate values of the deflections and bending moments along line 1-1 (at $y = 2$) and line 2-2 (at $y = 0$), respectively, for the cases $L_x = L_y = 0.4, 0.1, 0.05\,\text{m}$. It can be seen that

1. As the size of the column dimensions decreases, both results of the FEM and BEM become very close. This is mainly due to the modelling of columns in both methods being similar: in the FEM, each column is represented using frame element connected to the slab at single node and in the BEM the connection between the column and the slab is represented using very small cell ($0.05 \times 0.05\,\text{m}$).
2. Peak values over the columns in the finite element analysis are mainly due to the use of fine discretization in the FEM analysis. Unlike to the popular belief, such values do not affect the positive filed moment, which confirms the conclusion of Reference [6]. It has to be noted that such peaks do not appear in the present BEM analysis, when the real cross section of the column is taken into account.

In order to show the effect of the column cross-section geometry on the transferred moment from slab to the column, the following two analyses are carried out:

1. Using square columns ($L_x = L_y$) and varying L_x from 0.05 to 2 m:

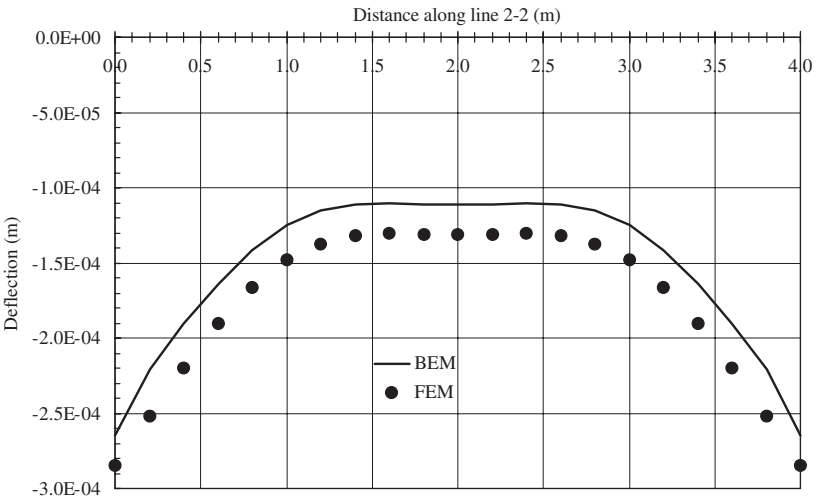

Figure 13. Deflection distribution along line 2-2 ($t = 0.4$).

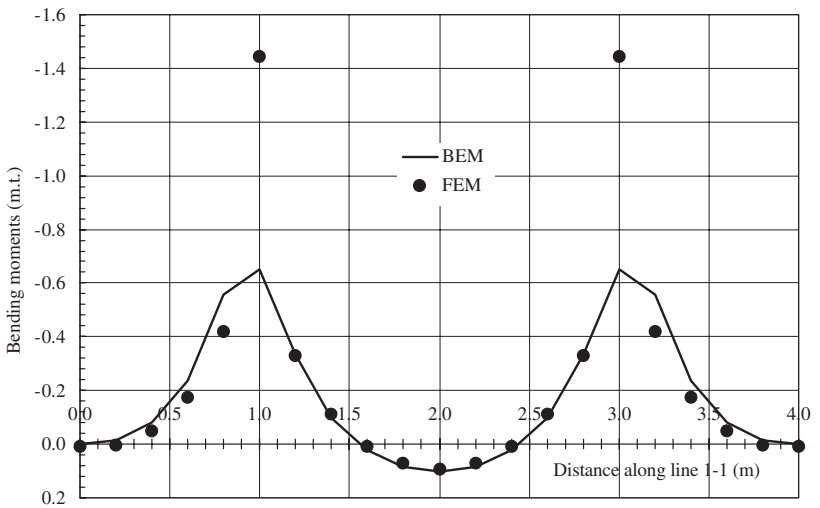

Figure 14. Bending moment diagram along line 1-1 ($t = 0.4$).

Figure 24 demonstrates values of bending moments carried by each column against L_x. Results are plotted from both the FEM and the present BEM solutions. It can be seen that after a certain value of the column width (0.8 m), the value of the transferred moment obtained from the FEM becomes constant (i.e. the FEM does not undergo any change in column geometry); whereas, in the BEM analysis, the value of such moment is decreased until it reaches zero when the column width $L_x = 2$ m. This is true as in this case the problem can be considered as a one-dimensional compression problem with no bending moments.

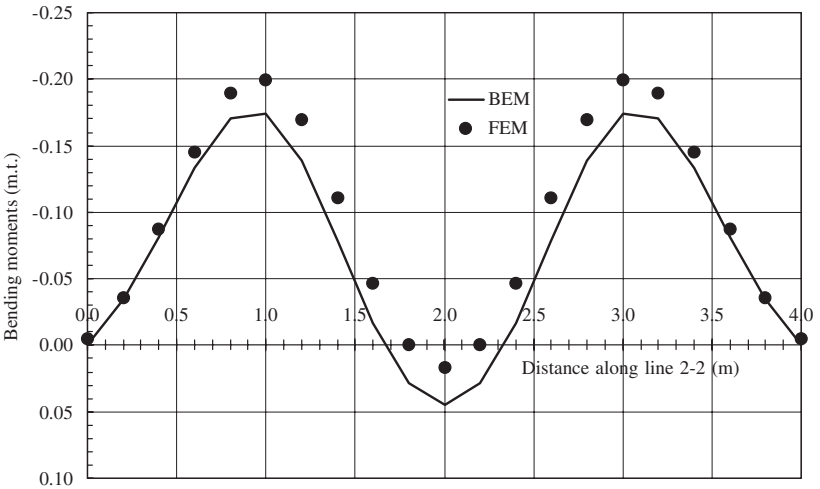

Figure 15. Bending moment diagram along line 2-2 ($t = 0.4$).

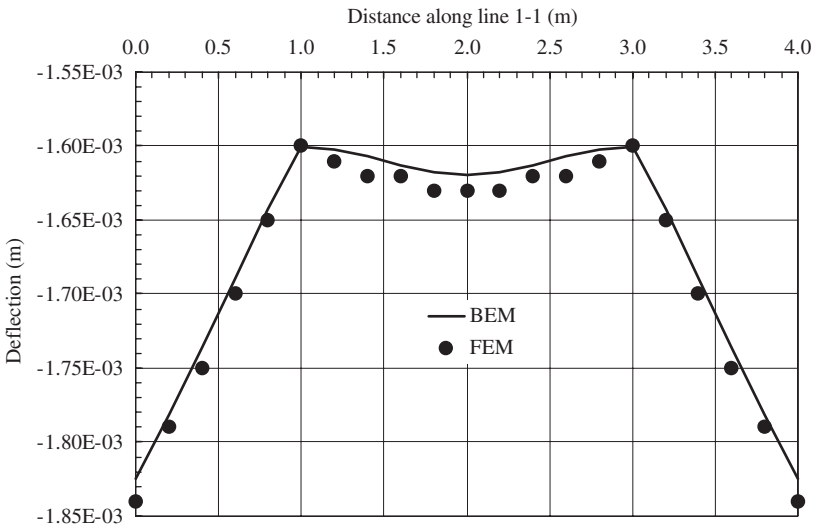

Figure 16. Deflection distribution along line 1-1 ($t = 0.1$).

2. Using rectangular columns by fixing $L_y = 0.05$ m, varying $L_x = 0.05$–2 m:

Figures 25 and 26 demonstrate the change of the column moment M_{yy} and M_{xx} by changing L_x. The following notes could be drawn from such figures:

1. A good agreement between the FEM and BEM results for the bending moment M_{yy}, which is the bending moment in the direction of the column short dimension. As in both the FEM and BEM models, the column connection to slab is modelled using either single node in the FEM or very small length ($L_y = 0.05$ m) in the BEM.

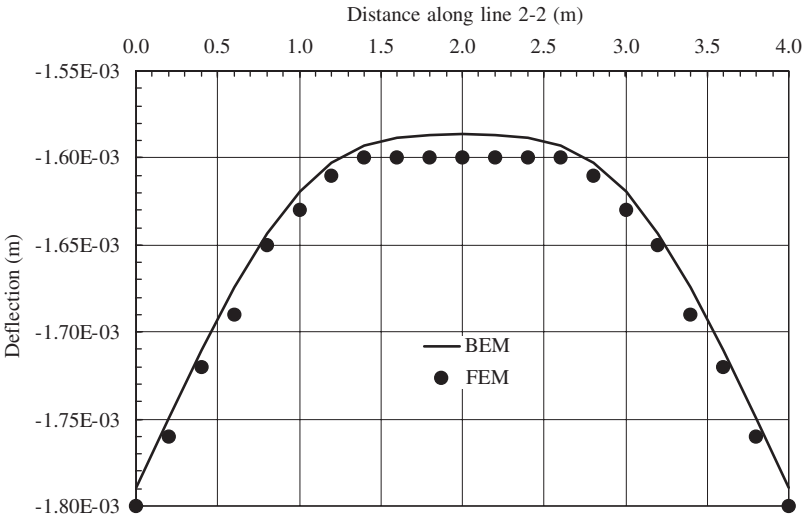

Figure 17. Deflection distribution along line 2-2 ($t = 0.1$).

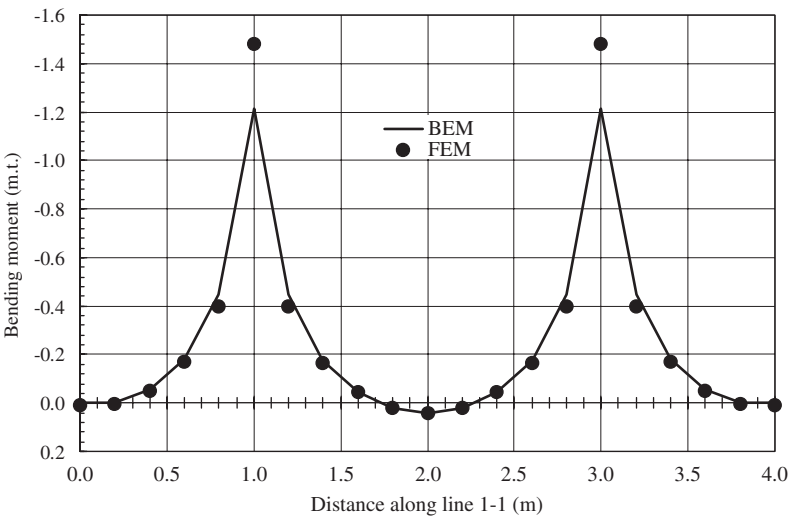

Figure 18. Bending moment diagram along line 1-1 ($t = 0.1$).

2. In the column long direction, as the length L_x increases the column stiffness increases and can attract more bending moment. This is true, until columns became long enough in a certain direction and in this case the slab behaves as a one-way slab that carries the load in the short direction; hence, the value of the bending moment decreases. It can be seen that such a point could not be observed in the FEM. This conclusion confirms the experimental results presented in Reference [4].

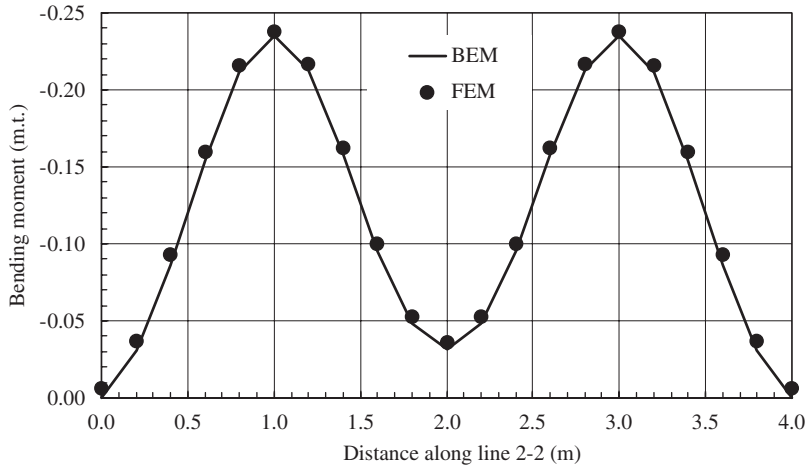

Figure 19. Bending moment diagram along line 2-2 ($t = 0.1$).

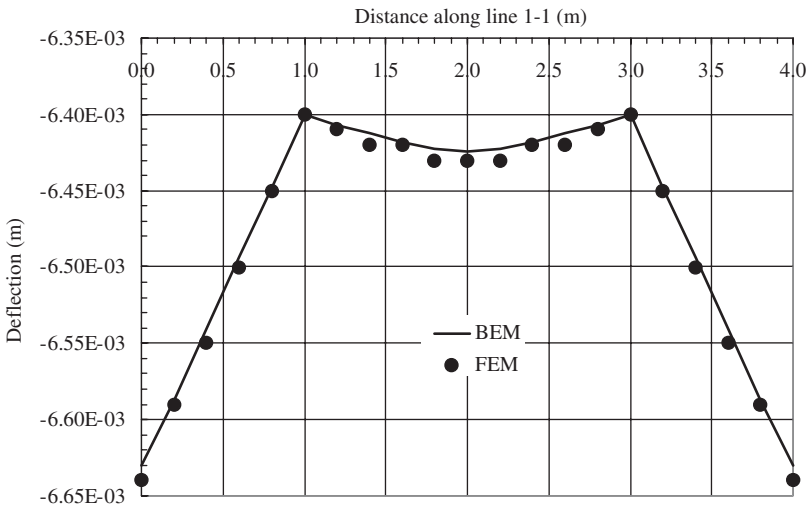

Figure 20. Deflection distribution along line 1-1 ($t = 0.05$).

6.3. Application to practical building slab

As it can be seen from the former example, the realistic geometry representation of the column cross-section could greatly affect the value of the bending moment transferred from the slab to the column, even in simple cases. In this example, such a conclusion will be confirmed for a problem with larger scale. The present example demonstrates also the use of the present formulation in the analysis of practical building floors and the results are compared to results obtained from finite element analysis packages, which are commonly used in structural design offices. The results presented here will be considered for both the field bending moment on the floor slab and the bending moment transferred from the slab to the columns.

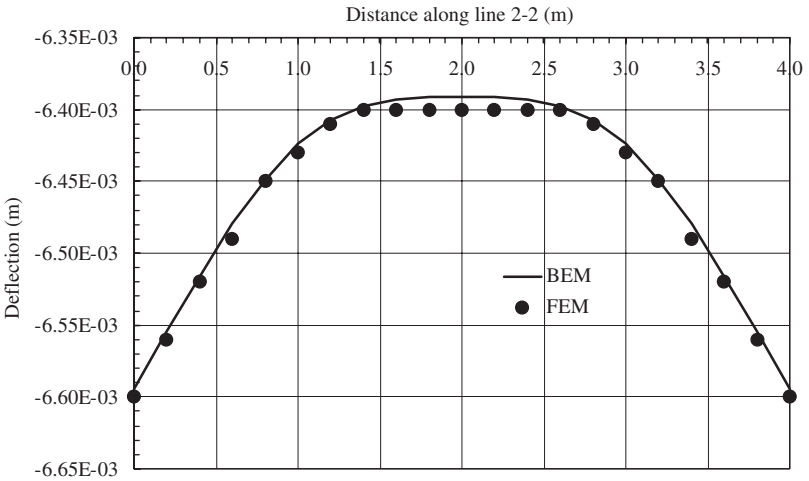

Figure 21. Deflection distribution along line 2-2 ($t = 0.05$).

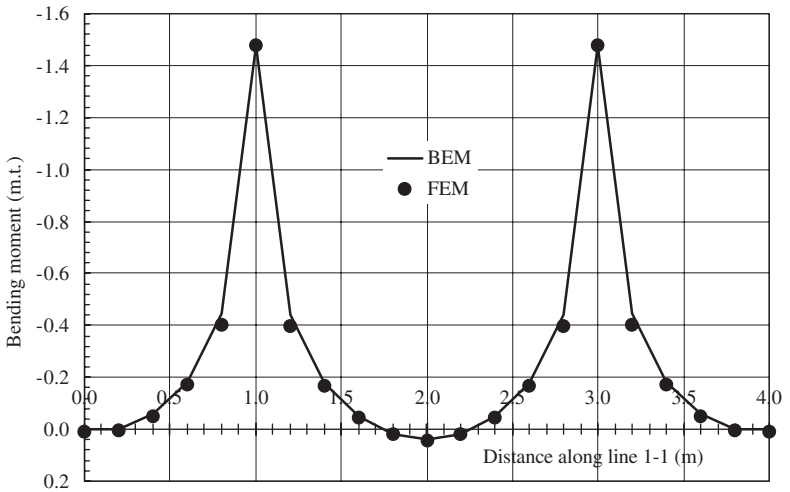

Figure 22. Bending moment diagram along line 1-1 ($t = 0.05$).

Consider the building shown in Figure 27. The building is of 23×21 m in plan, and has 19 columns. The slab of 0.3 m thickness and the following properties of reinforced concrete is used: $E = 2.1 \times 10^6$ t/m^2 and $v = 0.16$. The slab is analysed under vertical loading of -1.1 t/m^2. Table I shows the used column cross-sectional models. The heights of columns are 3 m and 3 m for the top and bottom floors, respectively.

The considered slab is analysed using the present boundary element formulation and also analysed using two different finite element meshes. In the finite element mesh 1 (see Figure 28), the slab is divided using 1×1 four-noded rectangular thick plate-bending element

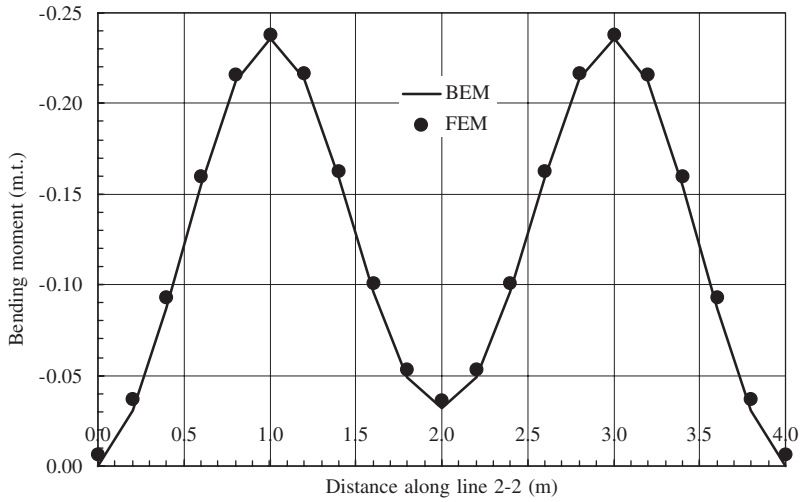

Figure 23. Bending moment diagram along line 2-2 ($t = 0.05$).

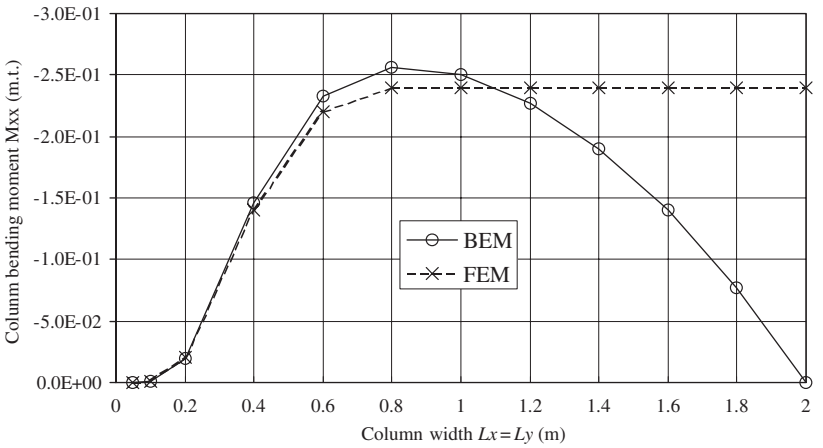

Figure 24. Changing of column bending moment M_{xx} by increasing L_x (and L_y) for square column dimensions.

(some elements were modelled using triangular elements to fit the inclined boundary). A total of 433 elements are used. Columns are modelled using the skeletal frame elements connected to the slab at single node and fixed at the top and bottom floor levels. The columns are connected to the slab at a single node. Mesh 2, on the other hand, has the same specifications as those of mesh 1, but it has 1727 elements, as shown in Figure 29.

In the boundary element analysis, the slab is divided into 109 quadratic boundary elements (each of 1 m in length; except for the elements along the inclined part of the boundary) and each column is modelled using its the real cross-section. The discretization of this mesh is depicted in Figure 30.

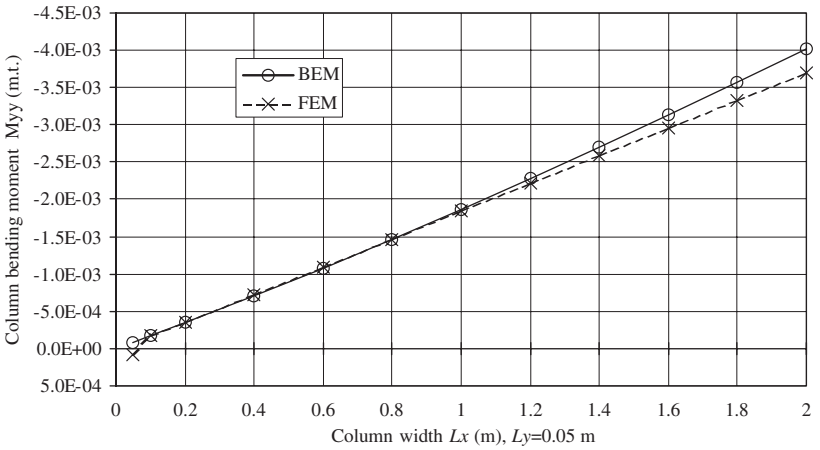

Figure 25. Changing of column bending moment M_{yy} by increasing L_x (L_y is constant = 0.05 m) for square column dimensions.

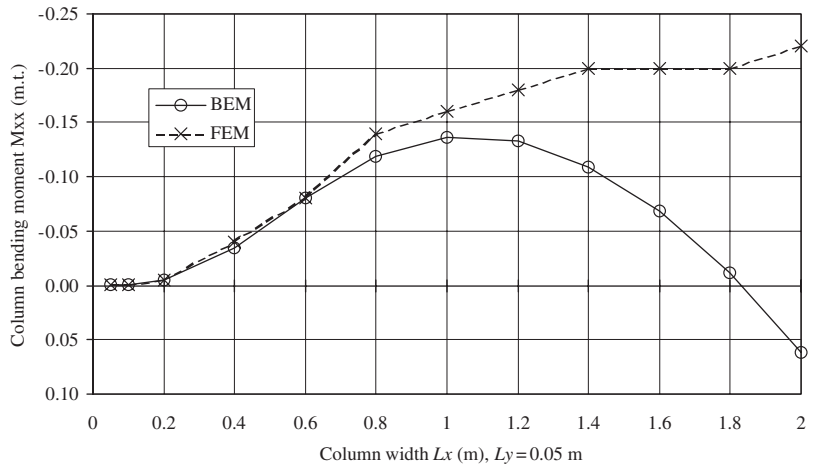

Figure 26. Changing of column bending moment M_{xx} by increasing L_x (L_y is constant = 0.05 m) for square column dimensions.

Table II shows the column bending moments and loads obtained from both the present BEM analysis and the two FEM analyses (using mesh 1 and mesh 2). The following notes could be written from the results shown in Table II:

1. The values of the vertical load carried by the columns are in excellent agreement between the present BEM analysis and both the FEM analyses.
2. Values of the bending moments for the columns are sometimes different; especially for bending moment M_{yy} as most of the columns have their long dimension along the y-axis.

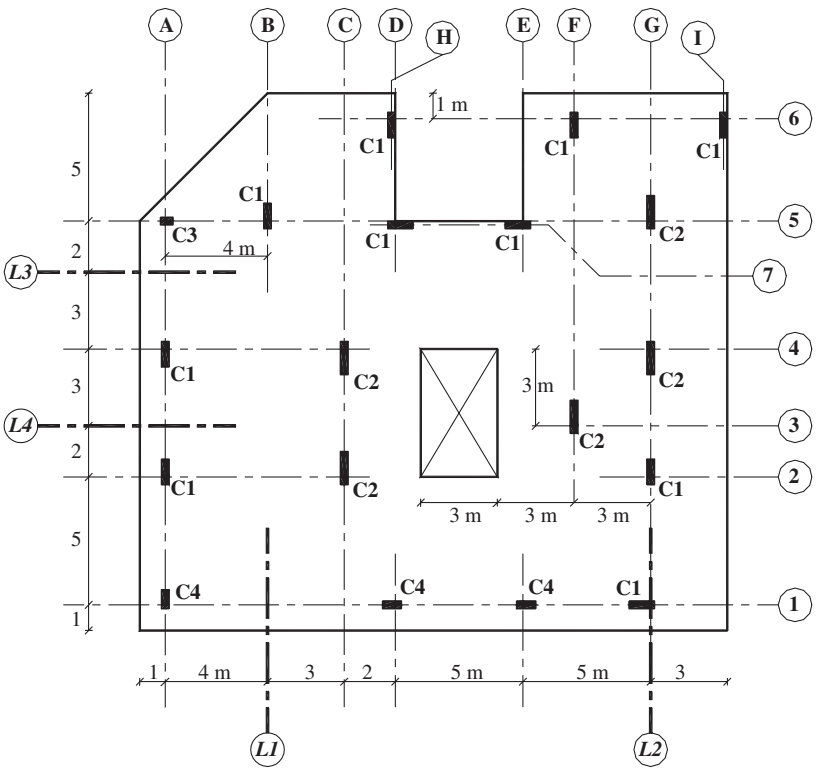

Figure 27. Geometry of the building slab considered in example 3.

Table I. Dimensions of used column models for the analysed problem in example 3.

Column model	Dimensions (m)
C1	0.3×1.00
C2	0.3×1.30
C3	0.3×0.50
C4	0.3×0.75

For example, columns G4 and C2 show large differences. It is very difficult to set up a rule or even to find numerical formulae to modify values obtained from FEM for the bending moments carried by the columns, as these values are highly dependent on several factors including the geometry and mechanical properties of the analysed problem. It can be seen that the only way to obtain accurate values is via carrying out the present BEM analysis.

Field deflections and bending moments, on the other hand, for the slab are plotted in Figures 31–38 along lines 1-1 to 4-4 (recall Figure 27). The following remarks could be

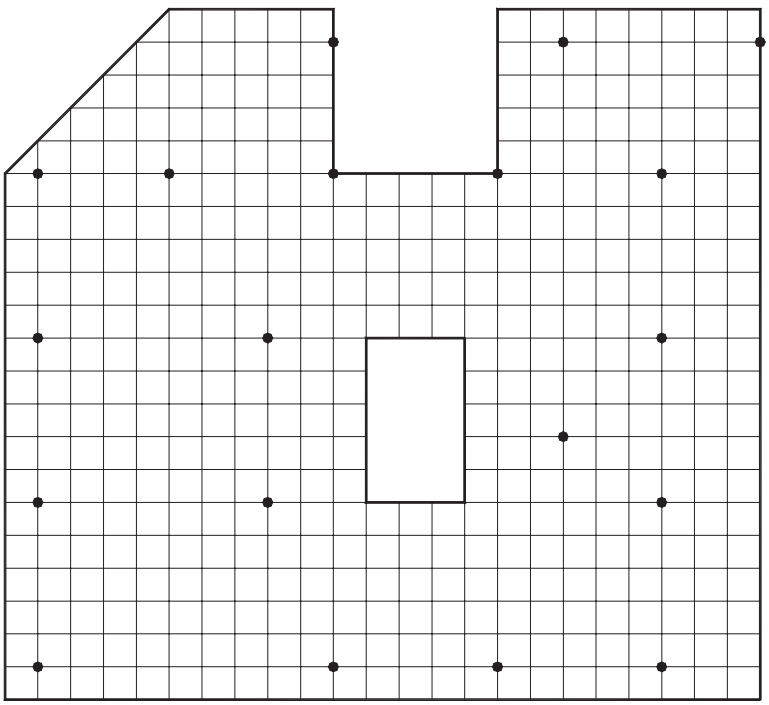

Figure 28. The finite element mesh (mesh 1) used in example 3.

observed:

1. The result values of the FEM analysis are not significantly affected by improving the discretization from mesh 1 to mesh 2. Therefore, the plotted values shown in Figures 31–38 are given only for mesh 1; except in Figures 35 and 36, values are shown for both meshes 1 and 2.
2. It can be seen that the slab deflection over columns in the present BEM demonstrates rigid zones, which represent column rigidity. Such representation cannot be observed in the corresponding FEM analysis.
3. Generally the computed deflections from the BEM results are less than that of the FEM analysis. This is mainly due to the consideration of the column real cross-section and the slab as continuum plate in the BEM analysis.

7. CONCLUSIONS

The present paper dealt with the analysis of flat plate building floors. The formulation presented can be considered practical and might be used among structural engineers. The boundary element method is used in modelling the field slab, where the effect of the shear deformations

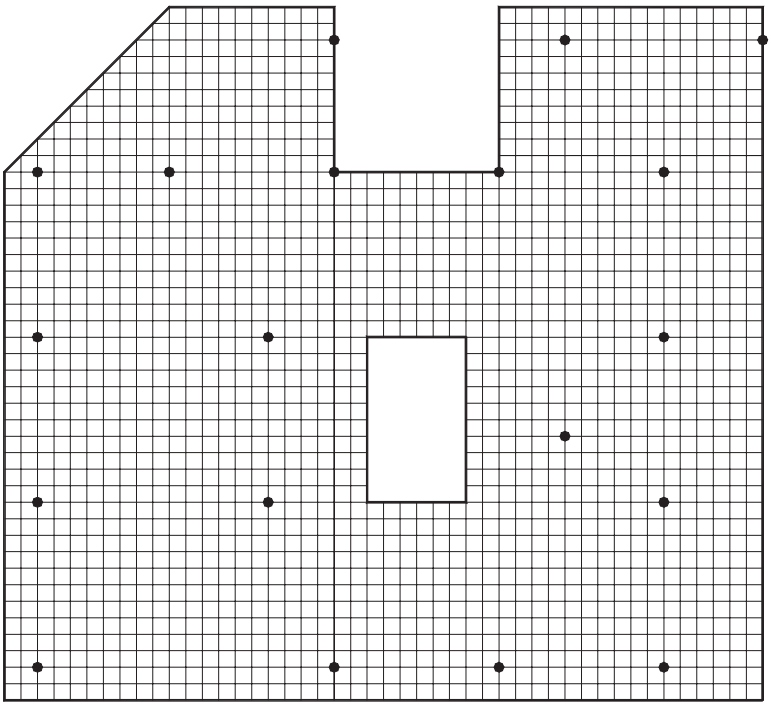

Figure 29. The finite element mesh (mesh 2) used in example 3.

is considered. Columns, walls or cores are modelled using their real cross-section. From the analysis presented and the results obtained from numerical examples, the following conclusions may be drawn:

1. The present BEM formulation as it can analyse any general slab with any boundary condition.
2. The formulation presented in this paper gains the following advantages:
   - Only the slab boundary is discretized, which is very suitable for complicated geometries. Re-analysis and testing of several design alternatives could be easily carried out.
   - The real dimensions of the internal supports (columns or walls) are considered, leading to more accurate results; especially for bending moments transferred from the slab to the columns.
   - The results can be computed anywhere inside the slab as post-processing procedures. Unlike most of BEM formulations presented in the literature, the present formulation can easily compute the values of deflections and bending moments over the columns.
   - The present formulation can compute the values of bending moments over columns without moment redistribution, which is usually needed when using the FEM.
   - The present formulation employs the shear deformation plate bending theory, which can be considered as more accurate for modelling of slabs.

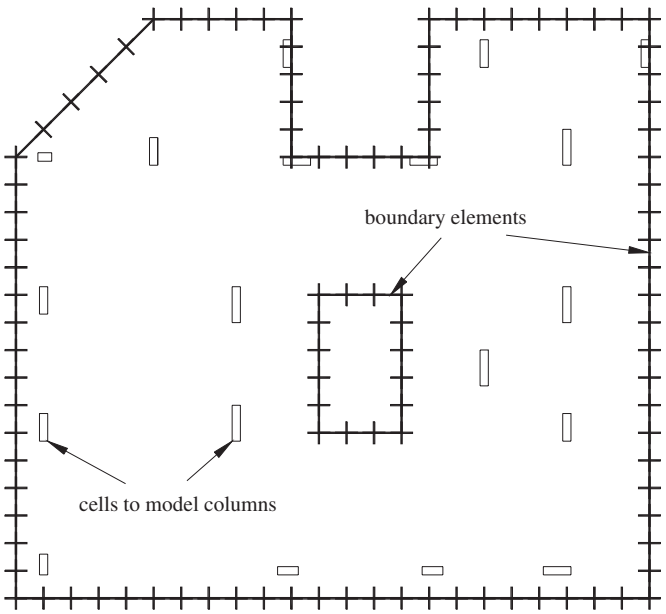

Figure 30. The boundary element mesh used in example 3.

Table II. Column bending moments and axial forces obtained from the FEM and BEM for the analysed problem in example 3.

	M_{xx} (m.t.)			M_{yy} (m.t.)			F (tonne)		
Column	BEM	FEM(1)	FEM(2)	BEM	FEM(1)	FEM(2)	BEM	FEM(1)	FEM(2)
I6	3.52	3.76	3.58	2.65	2.74	2.40	9.75	9.82	9.62
F6	−1.46	−1.92	−1.86	0.33	1.14	1.34	14.12	13.76	13.70
D6	9.35	9.88	9.32	−2.50	−2.08	−1.50	11.71	11.56	11.66
G5	−1.85	−1.96	−1.80	6.84	−2.60	2.08	29.05	29.68	30.00
E5	−4.12	−3.24	−3.32	8.77	8.14	7.72	23.82	25.04	24.88
D5	3.05	3.78	3.40	6.71	5.56	5.42	18.42	19.38	18.82
B5	−0.35	−0.06	−0.10	−7.31	−8.88	−7.6	35.88	34.96	35.62
A5	−3.50	−3.98	−3.84	−0.22	−0.94	−0.90	12.76	13.46	13.30
G4	−4.83	−2.46	−2.12	−10.24	−3.24	−3.06	29.08	30.76	30.74
C4	−2.31	−3.00	−2.76	−4.72	1.10	0.62	39.47	40.90	40.96
A4	−6.86	−6.22	−5.96	−0.75	1.34	1.24	20.17	20.18	19.88
F3	10.52	9.86	8.94	−0.24	−1.48	−1.22	36.66	37.02	37.26
G2	−4.83	−4.80	−4.42	9.05	5.54	5.00	29.99	29.36	29.32
C2	−0.17	−0.01	0.17	12.27	5.26	4.56	46.44	48.26	48.70
A2	−9.67	−9.34	−8.98	1.73	0.66	0.62	21.67	23.10	23.08
G1	−10.55	−7.34	−6.66	−5.76	−5.04	−4.94	19.94	19.84	19.86
E1	2.51	1.28	1.18	−7.78	−7.18	−6.98	21.37	21.38	21.10
D1	7.03	6.92	6.18	−6.08	−5.26	−5.22	27.77	26.78	26.80
A1	−10.29	−9.74	−9.58	−3.37	−3.76	−3.72	19.15	18.34	18.26

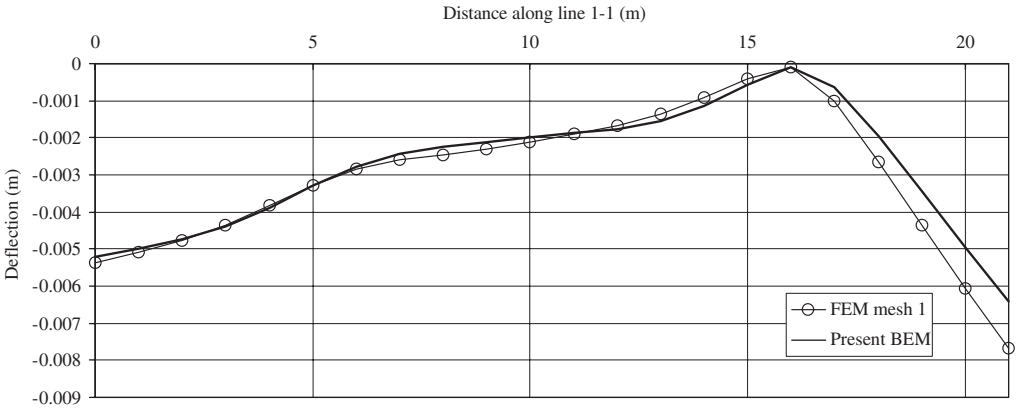

Figure 31. Deflection distribution along line 1-1.

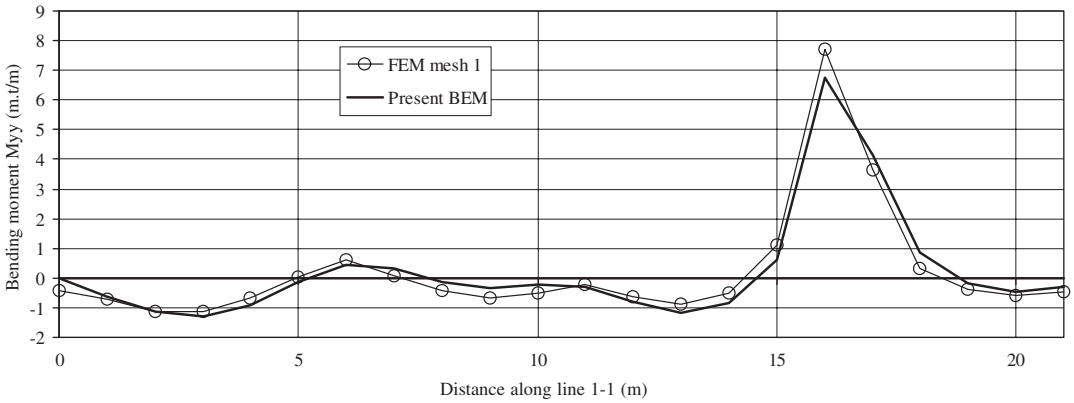

Figure 32. Bending moment M_{yy} distribution along line 1-1.

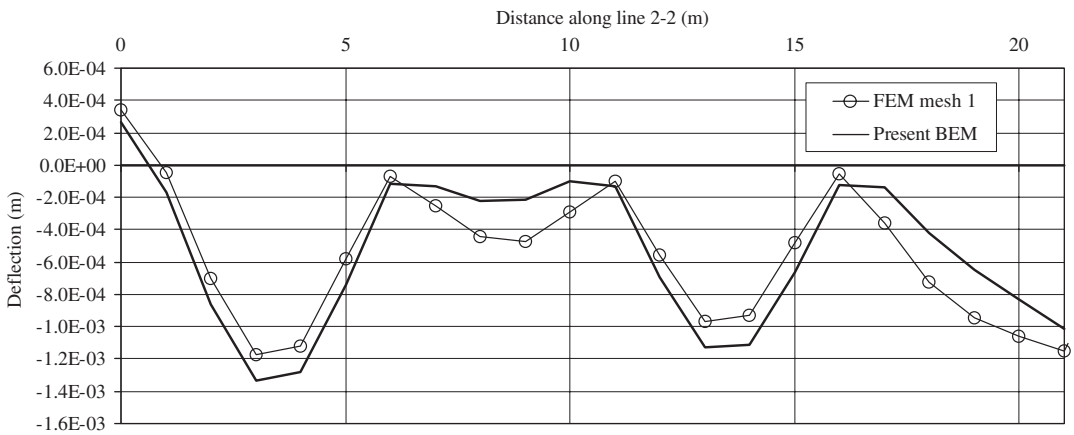

Figure 33. Deflection distribution along line 2-2.

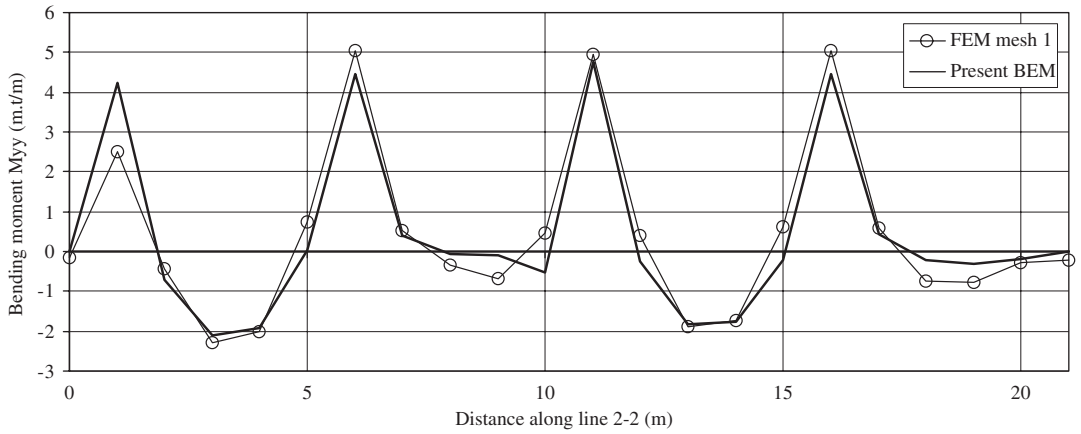

Figure 34. Bending moment M_{yy} distribution along line 2-2.

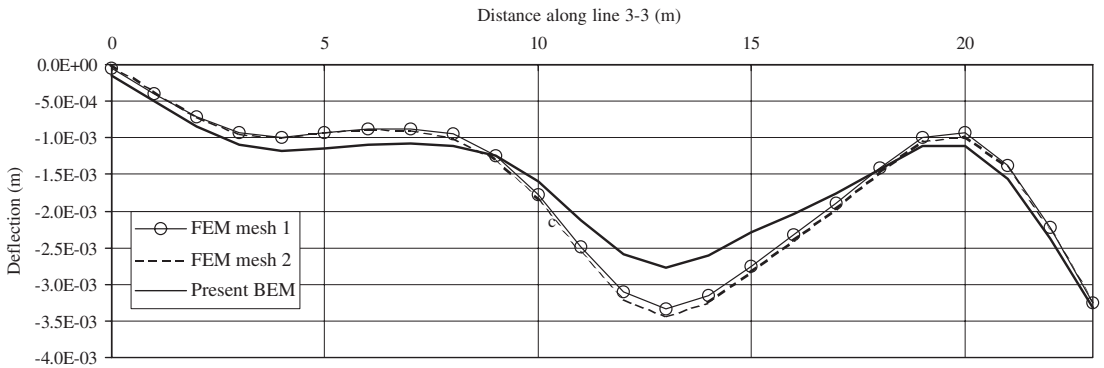

Figure 35. Deflection distribution along line 3-3.

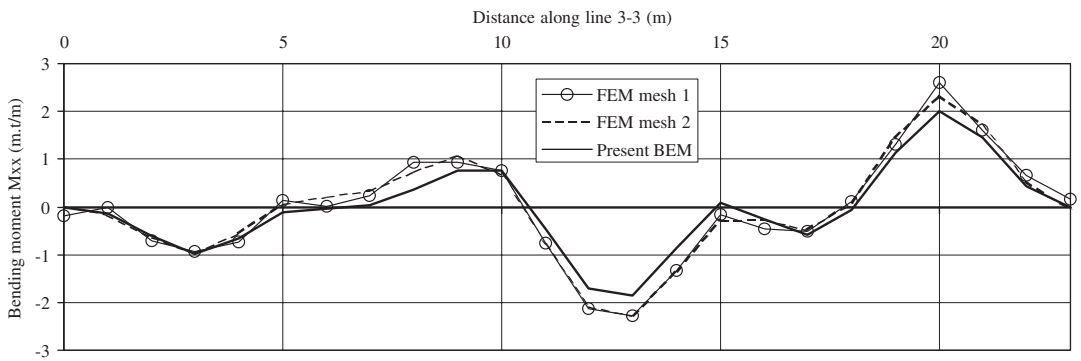

Figure 36. Bending moment M_{xx} distribution along line 3-3.

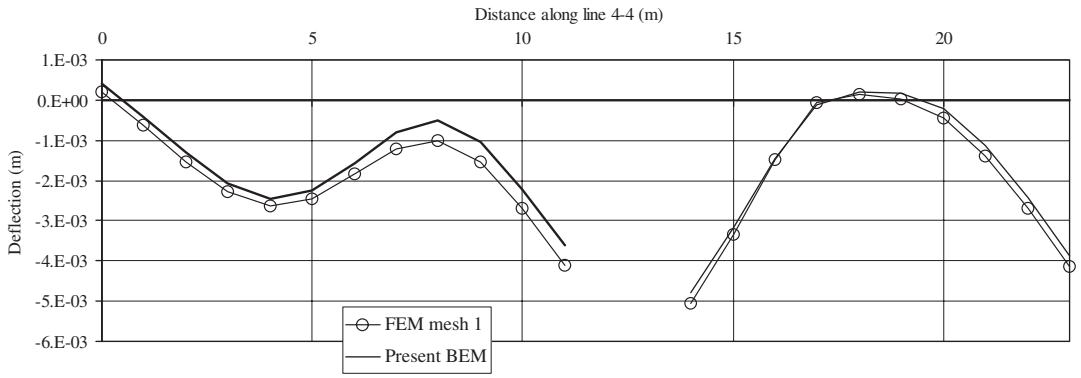

Figure 37. Deflection distribution along line 4-4.

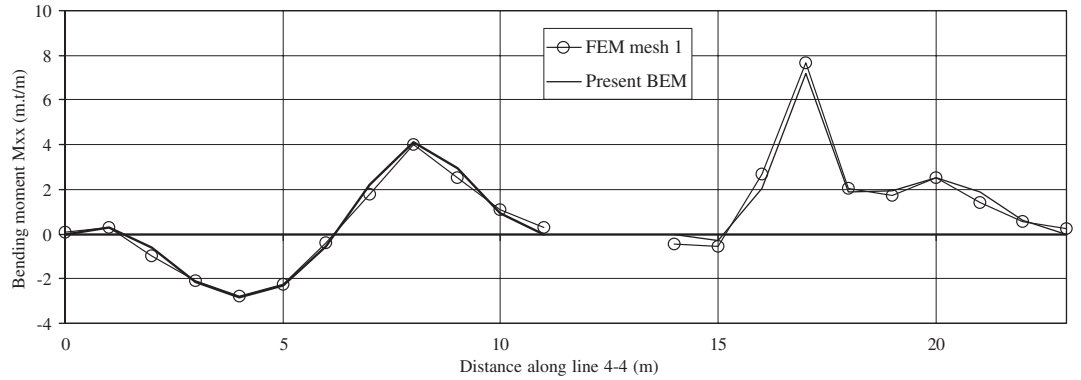

Figure 38. Bending moment M_{xx} distribution along line 4-4.

3. It has been demonstrated that the main difference between modelling flat plate floors using the FEM and BEM is the transferred moment from slabs to columns. Such values are greatly affected by considering the real dimensions of the columns cross-sections. Axial force carried by columns did not significantly differ in both the FEM and BEM.

A general conclusion of the present work is to recommend the present formulation to be used among engineers for more realistic modelling. It represents a robust alternative for available techniques that are commonly used among structural engineers and modellers.

Lateral load analysis of such structures and development of an end-user software based on the present formulation will be considered in the future work.

REFERENCES

1. Zienkiewicz OC. *The Finite Element Method* (3rd edn). McGraw-Hill: New York, U.K., 1977.
2. Hrabok MM, Hrudey TM. Finite element analysis in design of floor systems. *Journal of Structural Engineering* (ASCE) 1983; **109**(4):909–925.

3. Reissner E. On bending of elastic plates. *Quarterly of Applied Mathematics* 1947; **5**:55–68.
4. Simmonds SH. Flat slabs supported on columns elongated in plan. *ACI Journal* 1970; **67**:967–976.
5. Zaghw A, El-kafrawy M, Nasr M. The effect of column aspect ratio and marginal beams on the behaviour of R.C. flat slabs. *First Egyptian Structural Engineering Conference*, Cairo University, 1985; I/461–I/482.
6. Enochsson O, Dufvenberg P. Concrete slabs designed with finite element methods: modelling parameters, crack analysis and reinforcement design. *M.Sc. Thesis*, Lulea University of Technology, Sweden, October 2001.
7. Hillerberg A. *Strip Method Design Hand Book* (1st edn). Chapman & Hall Press: London, U.K., 1996, ISBN 0-419-18740-5.
8. Hillerberg A, Nylander H, Kinnunen S. Slabs. *Concrete Handbook—Design*. Chapter 6.5. AB Swensk Byggtjanst, Stockholm, Sweden, 1996, ISBN 91-7332-533-3.
9. Brebbia CA, Telles JCF, Wrobel LC. *Boundary Element Techniques*: *Theory and Applications in Engineering*. Springer: Berlin, Heidelberg, 1984.
10. Rashed YF. Applications of the boundary element methods in structural analysis and mechanics. *Engineering Analysis with Boundary Elements*, accepted.
11. Bézine G. Boundary integral formulation for plate flexure with arbitrary boundary conditions, *Mechanics Research Communications* 1978; **5**(4):197–206.
12. Stern M. A general boundary integral formulation for the numerical solution of plate bending problems. *International Journal of Solids and Structures* 1979; **15**:769–782.
13. Vander Weeën F. Application of the boundary integral equation method to Reissner's plate model. *International Journal for Numerical Methods in Engineering* 1982; **18**:1–10.
14. Bézine G. A boundary integral equation method for plate flexure with conditions inside the domain. *International Journal for Numerical Methods in Engineering* 1981; **15**:1647–1657.
15. Hartmann F. The boundary element method and Kirchhoff plates. In *BETECH85*, Brebbia CA, Noye BJ (eds). Computational Mechanics Publications: Southampton, UK, 1985.
16. de Paiva JB, Venturini WS. Analysis of building structures considering plate-beam-column interactions. In *Boundary Element Techniques*: *Applications in Stress Analysis and Heat Transfer*, Brebbia CA, Venturini WS (eds). Computational Mechanics Publications: Southampton, UK, 1987; 209–219.
17. de Paiva JB, Venturini WS. Boundary element algorithm for building floor slab analysis. In *BETECH85*, Brebbia CA, Noye BJ (eds). Computational Mechanics Publications: Southampton, UK, 1985; 201–209.
18. de Paiva JB. Boundary element formulation of building slabs. *Engineering Analysis with Boundary Elements* 1996; **17**:105–110.
19. de Oliveira Netoa L, de Paiva JB. A special BEM for elastostatic analysis of building floor slabs on columns. *Computers and Structures* 2003; **81**:359–372.
20. Hartley G, Abdel-Akher A. Analysis of building frames. *Journal of Structural Engineering* (ASCE) 1993; **119**(2):468–483.
21. Hartley GA. Development of plate bending elements for frame analysis. *Engineering Analysis with Boundary Elements* 1996; **17**:93–104.
22. Rashed YF. A coupled BEM-flexibility force method for bending analysis of internally supported plates. *International Journal for Numerical Methods in Engineering* 2002; **54**:1431–1457.
23. Telles JCF. A self-adaptive coordinate transformation for efficient numerical evaluation of general boundary element integrals. *International Journal for Numerical Methods in Engineering* 1987; **24**:959–973.

